Journal of Materials Chemistry C

ROYAL SOCIETY OF CHEMISTRY

PAPER

View Article Online
View Journal | View Issue



Cite this: J. Mater. Chem. C, 2023, 11, 6607

# An efficient hierarchical self-assembly approach to construct structurally diverse two-step sequential energy-transfer artificial light-harvesting systems†

Pei-Pei Jia,[a] Lianrui Hu,*[a] Wei-Tao Dou,[a] Xing-Dong Xu,[b] Haitao Sun,[c] Zhi-Yong Peng,[a] Dan-Yang Zhang,[a] Hai-Bo Yang[a] and Lin Xu*[a]

Received 10th December 2022,
Accepted 27th April 2023

DOI: 10.1039/d2tc05264d

rsc.li/materials-c



Efficiently fabricating artificial light-harvesting systems (LHSs) with cascade energy transfer properties is significant for mimicking natural photosynthesis. Through a coordination-driven self-assembly approach, metallacycle **M** surrounded by alkyl chains was successfully constructed from tetraphenylethylene (TPE) building blocks in nearly quantitative yield. Interestingly, from the prepared metallacycle **M**, star-shaped supramolecular complex **M-3** and cross-linked supramolecular network **M-4** with one-step energy-transfer properties were efficiently fabricated based on host–guest interactions. Furthermore, from **M-3** and **M-4**, two different artificial light-harvesting systems (LHSs) with two-step sequential energy transfer characteristics were efficiently prepared *via* supramolecular interactions. The two types of LHSs were compared in detail, and the critical factors affecting the light-harvesting efficiency, including the photophysical properties, aggregation-induced emission characteristics, energy transfer efficiency, and antenna effect, were carefully analysed. Additionally, both of the artificial LHSs, **M-3-5** and **M-4-5**, showed excellent energy transfer efficiency and high antenna effects. This research provides an efficient hierarchical self-assembly approach to construct artificial LHSs featuring excellent energy transfer efficiency and high antenna effects with diverse architectures.

## Introduction

The energy crisis is a global problem and searching for clean and economical energy sources is a global challenge. However, the sunlight reaching Earth every hour contains more energy than humans use in an entire year.[1] Widespread in nature, photosynthesis is a highly efficient process for capturing, transmitting, and storing light energy from the sun.[2] This process occurs in chloroplast pigments with highly efficient photon harvesting abilities owing to the large number of closely packed chlorophylls within the pigment–protein complexes. After transmitting through the chlorophyll molecules, the excitation energy is eventually transported to the reaction centre, where it is transformed into chemical energy.[3] Many scientists have attempted to solve the energy crisis by taking inspiration from photosynthesis.[4] In particular, much effort has been made to explore its complex mechanism and mimic its critical steps in recent decades.[3,5] To date, by mimicking the primary step of natural photosynthesis for efficiently utilizing light energy, a variety of artificial LHSs have been successfully designed and constructed for use in photocatalysis, biological imaging, and optoelectronic devices.[6]

Two important factors must be considered to construct an optimal artificial LHS: (1) the system must have several donors per acceptor, and (2) the donor must be tightly packed but free of aggregation-caused quenching (ACQ). Unfortunately, conventional chromophores tend to aggregate at high concentrations, which is detrimental to photoluminescence and results in undesired ACQ.[7] Therefore, exploiting strategies to increase chromophore density while minimizing self-quenching is still a major challenge in constructing LHSs. To date, the reported artificial LHSs constructed by covalent synthetic strategies have always faced multistep synthesis issues,[8] which prevent their scale-up and widespread application. Efficient natural LHSs

[a] Shanghai Key Laboratory of Green Chemistry and Chemical Processes, Shanghai Frontiers Science Center of Molecule Intelligent Syntheses, Wuhu Hospital Affiliated to East China Normal University, School of Chemistry and Molecular Engineering, East China Normal University, Shanghai 200062, P. R. China. E-mail: lrhu@chem.ecnu.edu.cn, lxu@chem.ecnu.edu.cn

[b] School of Chemistry and Chemical Engineering, National Engineering Research Center for Colloidal Materials, Shandong University, Jinan, Shandong 250100, P. R. China

[c] State Key Laboratory of Precision Spectroscopy, East China Normal University, Shanghai 200062, P. R. China

† Electronic supplementary information (ESI) available: Methods and additional figures and tables. See DOI: https://doi.org/10.1039/d2tc05264d

have been constructed noncovalently from protein and chlorophyll. Therefore, in contrast to conventional artificial LHSs using covalent bonds, supramolecular LHSs prepared with noncovalent interactions are typically simple to construct and free from multiple syntheses.[9] In fact, various artificial LHSs, including supramolecular polymers,[9a,10] organogels,[11] biomaterials,[12] and organic–inorganic hybrid materials,[13] have been successfully prepared *via* noncovalent self-assembly. Additionally, most reported artificial LHSs only have a one-step direct FRET process from donors to acceptors, but the extremely effective natural LHS entails multichannel information communication.[14] To mimic natural LHSs and understand related structure–function correlations, establishing structurally diverse multistep sequential FRET systems for systematic analysis is of great interest.[15] However, to date, only a few reported approaches have succeeded in realizing efficient structurally diverse artificial LHS construction, so the efficient construction of structurally diverse artificial LHSs with outstanding multistep energy transfer efficiency and antenna effects remains challenging.

Owing to their easy synthesis, solution processability, and tuneable photophysical properties, research on supramolecular self-assembly has advanced significantly over the past few decades. In this context, based on the building block TPE with aggregation-induced emission (AIE) properties,[16] a supramolecular hierarchical self-assembly approach has been designed to efficiently construct structurally diverse artificial LHSs featuring outstanding energy transfer efficiency and ultrahigh antenna effects. To achieve this goal, we employed a 120° TPE-containing dipyridyl donor decorated with terminal nitrile-functionalized alkyl chains and a 120° diplatinum(II) ligand to fabricate a discrete regular hexagonal metallacycle **M** through coordination-driven self-assembly in nearly qualitative yield (Scheme 1). Based on the host–guest interactions between the prepared metallacycle and neutral pillar[5]arenes, a star-shaped supramolecular complex **M-3** and a cross-linked supramolecular network **M-4** with one-step energy transfer properties were efficiently fabricated. After introducing the hydrophobic fluorescent dye Nile Red **5** into the aggregation states of assembly **M-3** and **M-4** as a second acceptor, an LHS with a two-step sequential energy transfer property was obtained for both of them. The two LHSs were compared in detail, and the critical factors that affect the higher light-harvesting efficiency and value of the antenna effect were carefully analysed. This research presents an efficient hierarchical self-assembly approach to construct structurally diverse artificial LHSs with two-step sequential energy transfer properties and sheds new light on strategies to enhance the energy transfer efficiency and antenna effects in artificial LHSs.

## Experimental

### Synthesis

**Materials.** All reagents were of analytical purity and used without further treatment. TLC analyses were performed on silica-gel plates, and flash chromatography was conducted using silica-gel column packages. All air-sensitive reactions were carried out under an inert $N_2$ atmosphere.

**Synthesis of 1.** Compound **1a** (1.90 g, 2.67 mmol) and 4-pyridylboronic acid (1.92 g, 16.00 mmol) were added to a 200 mL Schlenk flask, and the flask was evacuated and refilled with $N_2$ three times. Then, freshly distilled toluene (80 mL), ethanol (20 mL), and aqueous $K_2CO_3$ (2.88 g, 21.36 mmol)

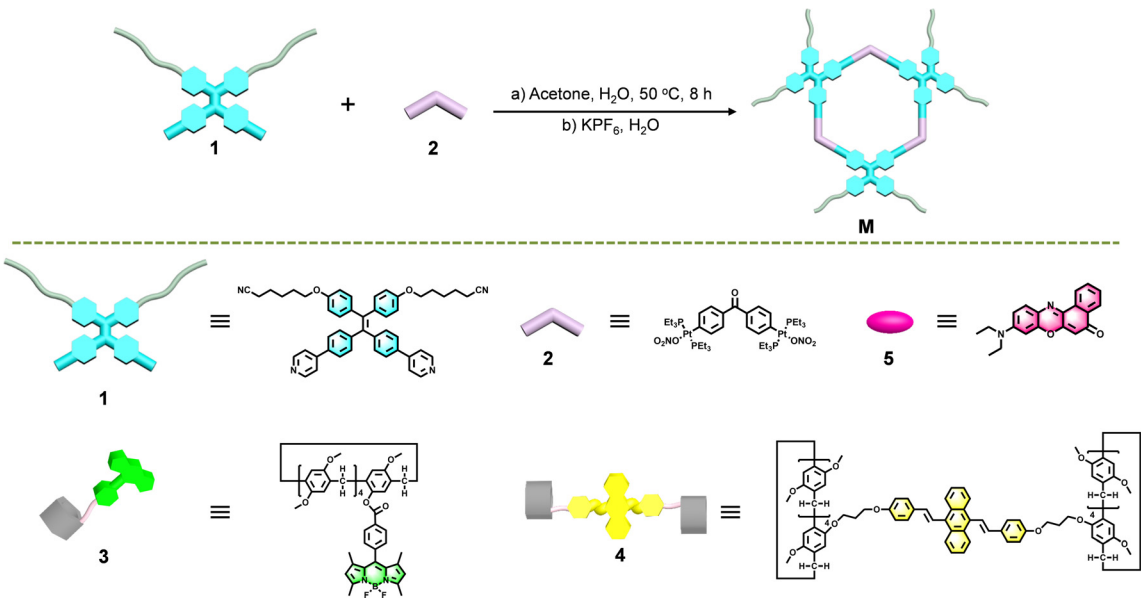


Scheme 1 Self-assembly of 120° dipyridyl donor **1** and 120° diplatinum(II) acceptor **2** into discrete hexagon metallacycle **M**. Chemical structures and cartoon representations of BODIPY-containing pillar[5]arene building block **3**, DSA-containing pillar[5]arene building block **4**, and fluorescent acceptor Nile Red **5**.

 

solution (20 mL) were added under nitrogen, $Pd(PPh_3)_4$ (601 mg, 0.52 mmol) was added, and the reaction mixture was stirred at 80 °C for 48 h under a nitrogen atmosphere. After cooling to room temperature, the product was concentrated and purified by flash column chromatography to afford compound **1** (820 mg, 43.4%) as a yellow powder.

**Synthesis of M.** **1** (12.63 mg, 17.82 μmol) and **2** (20.79 mg, 17.82 μmol) were mixed in a 1 : 1 molar ratio and dissolved in acetone/water (2.4 mL, 5/1, v/v). The whole reaction mixture was heated at 50 °C for 8 h to yield a homogeneous solution and then cooled to room temperature. Then, the addition of a saturated aqueous solution of $KPF_6$ into the bottle with continuous stirring resulted in product precipitation. The reaction mixture was centrifuged, washed several times with water, and dried. Then, a yellow powder was obtained.

### Characterization

UV-vis spectra were recorded in a quartz cell (light path 10 mm) on a Shimadzu UV2700 UV-visible spectrophotometer. Steady-state fluorescence spectra were recorded in a conventional quartz cell (light path 10 mm) on a Shimadzu RF-6000 fluorescence spectrophotometer (slit width 5 nm/5 nm for ex/em except for special instructions). The absolute fluorescence quantum yields were measured in solution using a commercial fluorometer with an integrating sphere (RF6000, Shimadzu). The fluorescence lifetimes were recorded in a quartz cell (light path 10 mm) on the Edinburgh FLS980 transient fluorescence spectrometer. All spectral measurements were made at room temperature.

### Computational methods

The extended tight binding (GFN2-xTB) semiempirical tight-binding method was employed to optimize the structures of TBC and TM in the gas phase with xtb software.[17] Then, the corresponding structure was rendered by VMD code.[18] The size was measured by means of Multiwfn software.[19]

## Results and discussion

It has been found that coordination-driven self-assembly, which is based on metal–ligand coordination interactions, is an effective method for creating discrete two-dimensional metallacycles and three-dimensional metallacages with accurate control over the shape and size of the final assemblies as well as the distribution and total number of incorporated functional moieties. The 120° TPE-containing dipyridyl building block **1** decorated with terminal nitrile-functionalized alkyl chain moieties was designed and synthesized through esterification and Suzuki–Miyaura coupling reactions (Schemes S1 and Fig. S1, S2, ESI†). Guided by the coordination-driven self-assembly approach, discrete regular hexagonal metallacycle **M** with three TPE molecules and six alkyl chains attached to the terminal nitrile was constructed in quantitative yield by stirring a mixture of 120° donor ligand **1** and 60° diplatinum(ii) acceptor **2** at a 1 : 1 molar ratio in acetone/water (5/1, v/v) (Scheme 1 and Scheme S2, ESI†). For efficient light collection in LHSs, a high-density array of chromophores is necessary. However, random aggregates of chromophores cannot be used because the excited state would be quickly quenched in the disordered aggregates by a process called ACQ.[6d,20] To address this ACQ effect, a TPE moiety with typical AIE properties was adopted to construct metallacycle **M** as the main building block. The obtained metallacycle **M** was first monitored by $^{31}P\{1H\}$ and $^{1}H$ NMR spectroscopy (Fig. S3–S5, ESI†).

Multinuclear NMR spectroscopy analysis confirmed that the formed metallacycle had a discrete and highly symmetric structure. For instance, the $^{31}P\{^{1}H\}$ NMR spectra of metallacycle **M** exhibited a sharp singlet at 14.22 ppm, which was shifted upfield by approximately 5.0 ppm relative to the starting 60° diplatinum(ii) acceptor **2**. This upfield shift and the decrease in the coupling of flanking $^{195}Pt$ satellites at approximately $\Delta J_{PPt} = -185.8$ Hz for **M** are consistent with back-donation from the platinum atoms (Fig. S6, ESI†). Additionally, significant downfield shifts were observed for metallacycle **M** in the $^{1}H$ NMR spectra compared to the proton signals of dipyridyl ligand **1**, resulting from the loss of electron density upon the coordination of the Pt(II) metal centre with pyridyl moieties (Fig. S7, ESI†). Moreover, the self-assembly of metallacycle **M** was further studied by 2D NMR techniques ($^{1}H$–$^{1}H$ COSY, $^{1}H$–$^{1}H$ NOESY, and DOSY), which proved the successful preparation of regular hexagonal metallacycle **M** (Fig. S8–S10, ESI†). ESI-TOF-MS analysis provided further support for the formation of a discrete and highly symmetric metallacycle. As shown in Fig. S11 (ESI†), the ESI-TOF-MS spectrum of metallacycle **M** exhibited three main peaks at $m/z$ = 1080.01, 1386.26, and 1896.66, corresponding to different charge states owing to the loss of the hexafluorophosphate counterions $[\mathbf{M} - 5PF_6^-]^{5+}$, $[\mathbf{M} - 4PF_6^-]^{4+}$ and $[\mathbf{M} - 3PF_6^-]^{3+}$, respectively, where **M** represents the initiating coordination architecture. More importantly, these peaks were isotopically resolved and were in good agreement with their theoretical distribution, which allowed the structure of the regular hexagonal metallacycle **M** to be definitely established. The structure of metallacycle **M** was also simulated by theoretical calculations, as shown in Fig. S12 (ESI†). Metallacycle **M** presented a roughly planar hexagonal ring with an internal diameter of approximately 3.4 nm and thus had a sufficient cavity for host–guest interactions.

Pillar[5]arene is capable of binding the neutral ditopic nitrile guest with strong affinity *via* host–guest interactions, according to previous reports.[21] The driving force of these host–guest processes mainly consists of dipole–dipole forces, hydrophobic effect, [C–H···π], [C–H···N], and [C–H···O] weak interactions with the addition of water. Hence, based on the host–guest interaction between pillar[5]arene and terminal nitrile-functionalized alkyl chains, a star-shaped supramolecular complex and a cross-linked supramolecular network were constructed from metallacycle **M** with BODIPY-decorated mono-pillar[5]arene and AIE-featured DSA-decorated di-pillar[5]arene, respectively. The self-assembly of metallacycle **M** with BODIPY-decorated mono-pillar[5]arene **3** to form star-shaped supramolecular complex **M-3** was first investigated by $^{1}H$ NMR spectroscopy. As indicated in Fig. S13 (ESI†), the related

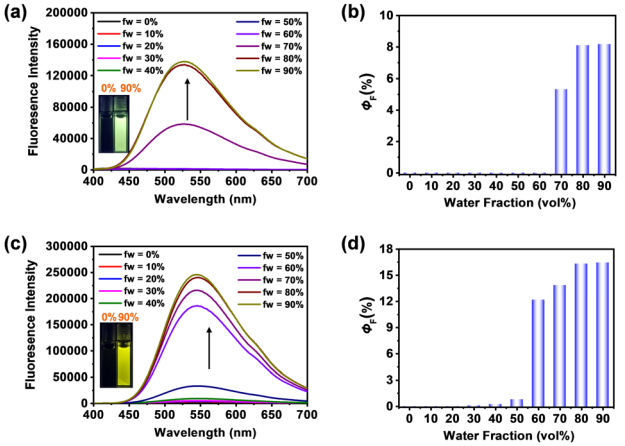


Fig. 1 Fluorescence emission spectra (a) and fluorescence quantum yields (b) of **1** *versus* the water fraction in the acetone/water mixtures (v/v). ($\lambda_{ex}$ = 365 nm, [TPE unit] = 20 μM). Fluorescence emission spectra (c) and fluorescence quantum yields (d) of **M** *versus* the water fraction in the acetone/water mixtures (v/v) ($\lambda_{ex}$ = 365 nm, [TPE unit] = 20 μM). Inset: Photographs of corresponding **1** (a) and **M** (c) *versus* the water fraction in the acetone/water mixtures (v/v) under a 365 nm ultraviolet lamp.

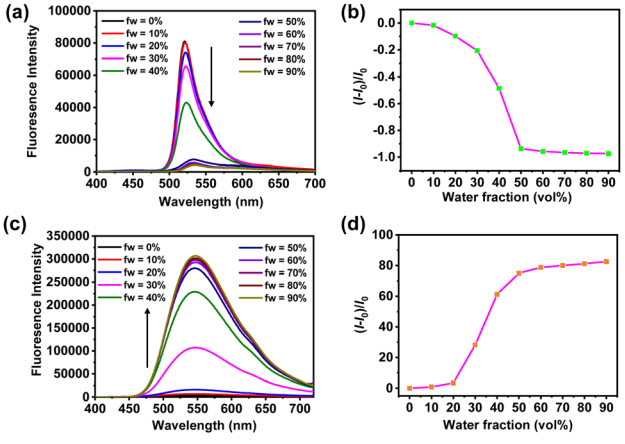


Fig. 2 Fluorescence emission spectra (a) and plots of $(I - I_0)/I_0$ (b) of **M-3** *versus* the water fraction in the acetone/water mixtures (v/v). Fluorescence emission spectra (c) and plots of $(I - I_0)/I_0$ (d) of **M-4** *versus* the water fraction in the acetone/water mixtures (v/v).

NMR signals of H1′–H5′ on metallacycle **M** showed obvious broadening and shifted upfield upon the addition of BODIPY-decorated mono-pillar[5]arene **3**. These chemical shift changes of the protons on guest metallacycle **M** indicated that the electron-rich cavity of pillar[5]arene was successfully filled by the guest molecule. Moreover, the host–guest interactions of metallacycle **M** and DSA-containing host **4** have also been characterized (Fig. S14 and S15), which proved the successful construction of host–guest complex **M-4**. Furthermore, the binding affinity of long-chain alkyl-CN-containing metallacycle **M** and pillar[5]arene ligands **3** or **4** was then evaluated to quantitatively evaluate the host–guest interactions. A 1 : 6 and 1 : 3 binding model were calculated in **M** : **3** and **M** : **4**, respectively, which were in accord with the existence of six long-chain alkyl-CN moieties of metallacycle **M** as guest binding sites and one pillar[5]arene of **3** as well as two pillar[5]arene of **4** as host binding sites (Fig. S16, ESI†). Due to the introduction of the TPE units, the AIE properties of ligand **1** and metallacycle **M** were investigated. As shown in Fig. 1(a) and (c), ligand **1** and metallacycle **M** were nonemissive in the acetone solution, and the emission intensity was dramatically enhanced with a water fraction close to 90%. The fluorescence quantum yield also showed a similar trend with the gradually increasing water fraction; thus, both ligand **1** and metallacycle **M** exhibited typical AIE properties (Fig. 1(b) and (d)). Notably, the fluorescence quantum yield of metallacycle **M** was approximately two times stronger than that of ligand **1**, showing typical AIE properties induced by metal–ligand coordination interactions. This change resulted from the coordination interactions between Pt–N bonds, which restricted the rotation of the phenyl groups on the TPE moieties.

Subsequently, with the combination of TPE-containing metallacycle **M** and BODIPY-containing pillar[5]arene **3** through host–guest interactions, the AIE properties of the assembled star-shaped supramolecular complex **M-3** were investigated. To construct the complex **M-3**, the molar ratio of metallacycle **M** and compound **3** was set to the optimal 1 : 6. As shown in Fig. 2(a) and (b), with a gradual increase in the water fractions in the acetone solution of complex **M-3**, the emission intensity of the system gradually decreased and showed a typical ACQ phenomenon. This may be due to the energy transfer process from TPE to the BODIPY moiety in the host–guest complex **M-3**, while the acceptor BODIPY is a typical ACQ molecule, so the fluorescence emission intensity gradually decreased with an increasing proportion of poor solvent water. Contrary to **M-3**, the AIE property of the cross-linked supramolecular network **M-4** was also measured, and typical AIE features were observed (Fig. 2(c) and (d)). When the water fraction in the acetone–water mixed solvent was less than 20%, the system exhibited dim fluorescence. The fluorescence emission signal was significantly enhanced as the water content increased from 20% to 50%. After the water fraction increased from 50% to 90%, the fluorescence intensity increased gradually, although the growth slowed dramatically. This was because the aggregation-caused restriction of molecular motion occurred at a water fraction of 20%. Under 365 nm irradiation from a UV lamp, the complex **M-4** system emitted bright yellow fluorescence. Compared with **M-3**, the fluorescence emission of **M-4** showed an opposite trend with an increase in the proportion of poor solvent, which was primarily attributed to the fact that both the TPE and the DSA moiety in **M-4** have AIE characteristics.

These investigations on the absorption and emission spectra of ligands, metallacycles, and host–guest complexes found that the emission spectra of **M** overlapped with the absorption spectra of both BODIPY- and DSA-decorated pillar[5]arenes **3** and **4**, respectively (Fig. S17, ESI†). Thus, it is possible to construct a FRET system by combining donor metallacycle **M** with BODIPY-decorated pillar[5]arene acceptor **3** and DSA-decorated pillar[5]arene acceptor **4** (Fig. 3(a) and (d)). It can be seen from the spectra (Fig. 3(b) and Fig. S18, ESI†) that as acceptor **3** was gradually added to the 90% acetone/water metallacycle **M** solution, the emission intensity of the whole

 

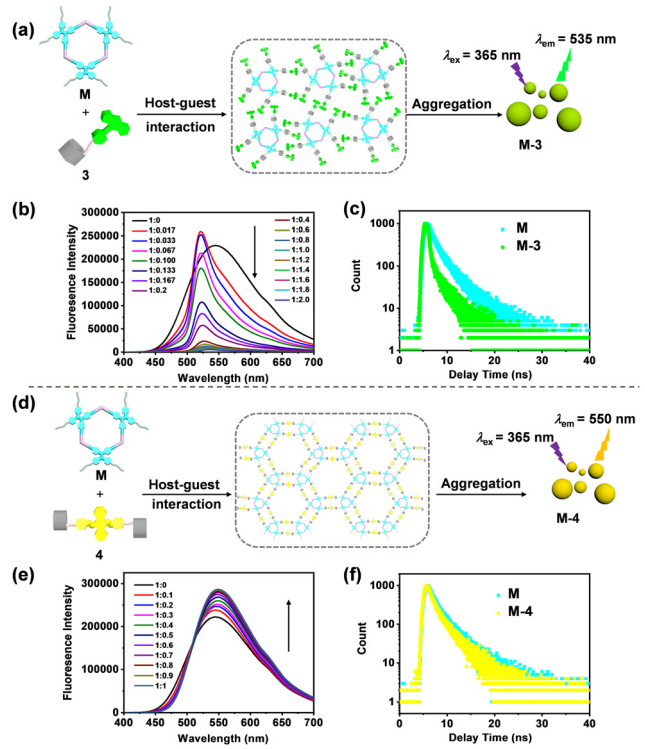


Fig. 3 (a) The fabrication of the FRET system between donor **M** and accepter **3**. (b) The fluorescence emission spectra of **M** with the addition of **3** in acetone/water (1/9, v/v) (c) The fluorescence lifetime of **M** and **M-3** in acetone/water mixtures (1/9, v/v) ($\lambda_{ex}$ = 365 nm, [TPE unit] = 20 μM, [BODIPY unit] = 40 μM). (d) The fabrication of the FRET system between donor **M** and accepter **4**. (e) The fluorescence emission spectra of **M** with the addition of **4** in acetone/water (1/9, v/v) ($\lambda_{ex}$ = 365 nm, [TPE unit] = 20 μM). (f) Fluorescence lifetime of **M** and **M-4** in acetone/water (1/9, v/v) ($\lambda_{ex}$ = 365 nm, [TPE unit] = 20 μM, [DSA unit] = 20 μM).

system steadily decreased. This might be attributed to the broad emission peak of the TPE moiety covering the whole emission peak of BODIPY. However, the emission peak assigned to the TPE moiety decreased obviously with the addition of acceptor **3**. This confirmed the successful energy transfer from the TPE moiety to the BODIPY moiety. As the percentage of acceptor **3** increased, the emission of the whole system was mainly attributed to the contribution of BODIPY; however, BODIPY is a typical ACQ molecule and caused substantial energy loss in the 90% water fraction solvent. The emission peak from the TPE moiety almost disappeared with a donor/acceptor ratio of 1 : 6 (Fig. S19, ESI†). Further fluorescence decay profiles also verified the FRET energy transfer from **M** to acceptor **3**. As shown in Fig. 3(c) and Table S1 (ESI†), the average lifetime of metallacycle **M** was 1.55 ns, and it decreased to 0.95 ns under the same measurement conditions after addition of acceptor **3** into the system. A similar energy transfer process was also successfully constructed by metallacycle **M** with DSA-containing acceptor **4** (Fig. 3(e)–(f), Fig. S20, S21 and Table S2, ESI†). Because the emission peak overlap between **M** and **4** was smaller than that of the energy transfer system constructed by **M** and **3**, the emission wavelength between 500 and 700 nm attributed to the DSA moiety gradually increased with the addition of acceptor **4**, which was accompanied by a decrease in the emission of donor metallacycle **M** at 400–500 nm upon excitation at 365 nm (Fig. S22, ESI†). These outstanding optical properties indicate that two first-order energy transfer systems, a star-shaped supramolecular complex and a cross-linked supramolecular network structure, were efficiently and separately constructed from metallacycle **M** through host–guest chemistry.

The morphologies and sizes of the formed aggregates of host–guest complex **M-3** and **M-4** in acetone/water (1/9, v/v) were investigated by dynamic light scattering (DLS) and transmission electron microscopy (TEM) measurements (Fig. S23a and 24a, ESI†). DLS experiments show that the **M-3** and **M-4** complex formed well-defined aggregates with a narrow size distribution, giving an average diameter of 93 nm and 224 nm, respectively. Additionally, both solutions exhibited an apparent Tyndall effect as further evidence of the existence of nanoaggregates. TEM experiments were carried out to determine the morphologies of the aggregates. According to Fig. S23a, 24a (ESI†), the obtained TEM images revealed several nearly spherical shapes with an average diameter of approximately 88 nm and 210 nm, which agrees with the corresponding DLS data. These results, combined with the excellent optical properties, showed the excellent capability of the **M-3** and **M-4** aggregates in acetone/water (1/9, v/v) to fabricate artificial LHSs.

Furthermore, a two-step sequential energy-transfer process was realized by simultaneously encapsulating another carefully selected hydrophobic dye as the second energy acceptor. To construct a two-step sequential FRET system, hydrophobic fluorescent dye **5** (Nile Red) was chosen as a promising acceptor because its absorption closely matched the emission of the aggregates of complex **M-3** and **M-4** (Fig. 4(a), 5(a) and Fig. S25, ESI†). The TEM images show roughly spherical forms with an average diameter of approximately 96 nm and 227 nm. In comparing with **M-3** and **M-4**, the average diameter of these two sequential FRET systems **M-3-5** and **M-4-5** had increased, indicating the Nile Red **5** was successfully constructed into both **M-3** and **M-4** systems. The DLS data also confirmed these results (Fig. S23b and 24b, ESI†). Then, the light-harvesting behaviour of star-shaped supramolecular complex **M-3** combined with fluorescent dye **5** was investigated. As acceptor **5** was incorporated into the **M-3** assembly, the emission band at 535 nm ascribed to the BODIPY chromophore on acceptor **3** gradually decreased, while the emission peak of acceptor **5** at 630 nm increased (Fig. 4(b)). In addition, as the receptor **5** ratio changed, it can be observed from Fig. 4(c) that the visual fluorescent colour changed from green-yellow to red. Based on the 1931 Commission Internationale de L'Eclairage (CIE) chromaticity diagram, the emission was mainly located in the red region ($CIE_x > 0.40$). The CIE chromaticity diagram also confirmed the change in fluorescence colour from green-yellow [CIE coordinate (0.42 : 0.54)] to red [CIE coordinate (0.63 : 0.37)] (Fig. 4(d)). When the ratio of donor **M-3** and acceptor **5** reached 1 : 6 : 0.067, an optimal secondary energy transfer efficiency of 40% was observed from the BODIPY chromophore moiety to

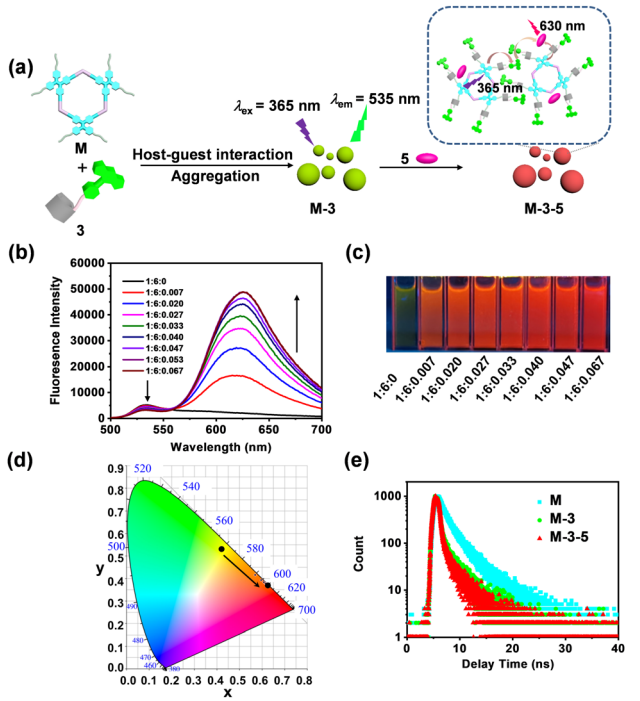


Fig. 4 Fabrication of artificial light-harvesting system **M-3-5** (a). The fluorescence emission spectra at 500–700 nm of **M-3** with the addition of **5** (b). Photographs (c) and CIE coordinates (d) of **M-3-5** in acetone/water (1/9, v/v) with different concentrations of **5** under a 365 nm UV lamp. The fluorescence lifetime of **M-3-5** in acetone/water (1/9, v/v) (e). ($\lambda_{ex}$ = 365 nm, slit (5 nm, 5 nm), [TPE unit] = 20 μm, [BODIPY unit] = 40 μM).

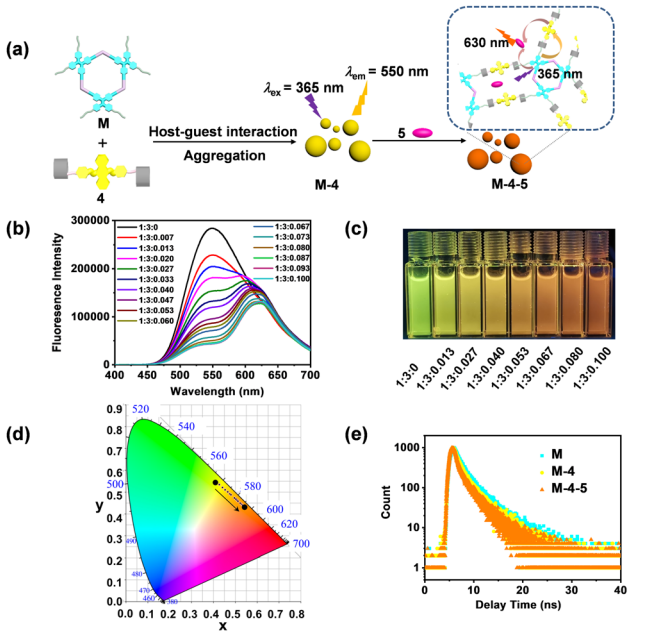


Fig. 5 Fabrication of the artificial LHS (a). Fluorescence emission spectra of **M-4** in acetone/water (1/9, v/v) with the addition of **5** (b). Photographs (c) and CIE coordinates (d) of **M-4-5** in acetone/water (1/9, v/v) with different concentrations of **5** under a 365 nm ultraviolet lamp. The fluorescence lifetime of **M-4-5** in acetone/water (1/9, v/v) (e). ($\lambda_{ex}$ = 365 nm, slit (5 nm, 5 nm), [TPE unit] = 20 μM, [DSA unit] = 20 μM).

Nile Red **5**, and the corresponding antenna effect was 4.1 (Fig. S26, ESI†). These observed phenomena suggested that the energy transfer process from **M-3** to **5** effectively occurred, and a supramolecular artificial LHS was successfully fabricated. Upon excitation with ultraviolet light at 365 nm, a decrease in the fluorescence lifetime from the aggregates of complex **M-3** ($\tau$ = 0.95 ns) to the LHS **M-3-5** ($\tau$ = 0.82 ns) was observed in the fluorescence decay experiments (Fig. 4(e)), indicating that secondary energy transfer occurred from **M-3** to **5** and providing additional evidence that light harvesting was successfully performed. Notably, all the above optical experiments were performed under UV light irradiation at 365 nm, and combined with the first-order energy transfer results from metallacycle **M** to **M-3**, all these optical results indicated that metallacycle **M** successfully served as a donor in the LHS. The two-step sequential energy transfer process took place from metallacycle **M** to acceptor **3** and then to Nile Red **5** in relay mode.

In addition, for comparison with the LHS constructed from **M-3** and to evaluate the efficiency of the presence of a TPE unit, AIE-featured cross-linked supramolecular network **M-4** was used to fabricate artificial LHSs in acetone/water (1/9, v/v) through the addition of acceptor **5** (Fig. 5(a)). It can be observed from the spectra (Fig. 5(b)) that with the gradual addition of acceptor **5** into the **M-4** system, the starting emission intensity at 550 nm decreased, while the emission peak at 630 nm ascribed to acceptor **5** increased first and then gradually decreased after **M-4-5** reached the optimal ratio of 1 : 3 : 0.020. As the receptor **5** ratio changed, a variety of emission colours were observed from green-yellow [CIE coordinate (0.41 : 0.54)] to orange [CIE coordinate (0.54 : 0.44)] (Fig. 5(c) and (d)). According to the fluorescence decay profiles (Fig. 5(e)), a decrease in the average fluorescence lifetime from **M-4** ($\tau$ = 1.28 ns) to **M-4-5** ($\tau$ = 1.17 ns) was observed, indicating that secondary energy transfer took place from **M-4** to **5** and providing additional evidence that the LHS of **M-4-5** was successfully fabricated. Specifically, all the above optical experiments were carried out under irradiation with UV light at 365 nm. When considered together with the first-order energy transfer results from metallacycle **M** to acceptor **3**, all these optical results indicated that metallacycle **M** successfully served as a donor in LHS, and the two-step sequential energy transfer process took place sequentially from metallacycle **M** to acceptor **4** and then to Nile Red **5**. Subsequently, the energy transfer efficiency and antenna effect were calculated to quantitatively evaluate the light-harvesting efficiency of the constructed LHS. According to the fluorescence spectra in Fig. S27 (ESI†), the secondary energy transfer efficiency was determined to reach 84.5%, and the antenna effect was estimated to be up to 10.1 for LHS **M-4-5** at a ratio of 1 : 3 : 0.10 (excitation at 365 nm). Compared with the secondary energy transfer efficiency of 40% and antenna effect of 4.1 from **M-3-5**, the LHS **M-4-5** constructed from AIE-featured DSA decorated di-pillar[5]arene was dramatically enhanced. Upon excitation with UV light at 365 nm, the energy transfer efficiency of LHS **M-4-5** was calculated to be 2.11-fold stronger than that of the LHS of **M-3-5** at a ratio of 1 : 6 : 0.067, and the

 

antenna effect was enhanced approximately 2.46-fold. As shown in Fig. S26b and S27b (ESI†), the fluorescence spectra upon excitation at 550 nm and the emission spectra upon excitation at 365 nm were similar for both assemblies **M-3-5** and **M-4-5**, demonstrating that both artificial LHSs also possessed an excellent ability to harvest visible green light. Additionally, under the same conditions, as **5** was incorporated into aggregation-based **M**, the emission band at 550 nm ascribed to the TPE chromophore on acceptor **5** gradually decreased. In comparison, the emission peak of acceptor **5** at 630 nm increased. These results demonstrated that energy transfer occurred from **M** to **5** in **M-5** but with an inferior antenna effect (Fig. S28, ESI†). These observed phenomena suggested that the energy transfer process from **M** to **5** occurred. Therefore, the **M-3-5** and **M-4-5** can provide an efficient FRET platform, which simultaneously exists three FRET processes. Moreover, density functional theory (DFT) calculations showed that the TPE has a larger energy gap of 3.96 eV between the lowest unoccupied molecular orbital (LUMO) and the highest occupied molecular orbital (HOMO) than the other three chromomere acceptors. The largest energy gap meant that TPE was easier to generate electron excitation under the shortest wavelength irradiation and be a more desirable energy donor. The LUMO energy of TPE is −1.59 eV. In comparison, the calculated LUMO energy for BODIPY and DSA were −2.62 eV and −2.20 eV, while NiR was only −2.72 eV, which meant that they were more prone to electron reception and were more desirable energy acceptors (Fig. S29 and S30, ESI†). These results indicate that the supramolecular artificial LHSs **M-3-5** and **M-4-5** could be an efficient platform for harvesting solar energy from the UV and green visible-light range, which provides an efficient strategy to mimic photosynthesis with high energy utilization.

Thus, through the strategy of hierarchical self-assembly, a star-shaped supramolecular complex and cross-linked supramolecular network were efficiently constructed. Both acted as artificial LHSs with high secondary energy transfer efficiency and antenna effects in the aggregation states. Notably, compared with star-shaped supramolecular complex **M-3-5**, cross-linked supramolecular network **M-4-5** exhibited a superior light-harvesting ability, which was mainly because the acceptor DSA-containing **4** in the **M-4-5** system was an AIE molecule. While BODIPY-containing acceptor **3** in the **M-3-5** system was an ACQ molecule, its luminescent performance in the aggregated state was poor, which is not conducive to light capture and transfer. These results also show that using molecules with AIE properties to construct light-harvesting systems has significant advantages. Additionally, the cross-linked supramolecular network formed a densely packed cross-linking structure, and the energy transfer efficiency between molecules was significantly higher, which may also be another reason for its better light-harvesting efficiency. Finally, by changing the ratio of receptor molecules **3** or **4** in the above two artificial LHSs, it was possible to achieve a variety of colour emission regulations from yellow-green to red or from yellow-green to orange, respectively, resulting in high potential application in luminescent materials.

# Conclusions

In summary, two structurally different supramolecular artificial LHSs were efficiently constructed from discrete hexagon metallacycle **M** by combining hydrophobic, host–guest, and coordination interactions. Based on the sequential FRET mechanism, both exhibited two-step sequential energy-transfer properties with excellent light-harvesting efficiency and a high antenna effect. Due to the excellent photoluminescent properties in the aggregation states compared to those of ACQ units, it was clear that using molecules with AIE features to construct light-harvesting systems increased their energy transfer efficiency and antenna effect. In comparison to the star-shaped supramolecular complex-based LHS **M-3-5**, the energy transfer efficiency of the cross-linked supramolecular network-based LHS **M-4-5** was enhanced approximately 2.11-fold, and the antenna effect was enhanced approximately 2.46-fold. In addition, by changing the ratio of the second acceptor Nile Red **5** in these two artificial LHSs, the emission colour was tuned from green-yellow to red or from green-yellow to orange, resulting in significant application potential in luminescent materials. Therefore, this study not only provides a unique approach driven by metal–ligand coordination interactions, host–guest interactions, and hydrophobic interactions for the efficient fabrication of structurally diverse multistep artificial LHSs with high energy transfer and antenna efficiency but also offers prospects for utilizing solar energy by artificial LHSs for the future production of renewable energy. Moreover, this research enriches our understanding of the structure–function correlations of artificial LHSs and the correlation with the photophysical processes therein, possibly leading to the realization of new types of solar power conversion devices incorporating a multistep sequential energy-transfer supramolecular artificial LHS.

# Author contributions

P.-P. Jia, L. Hu, W.-T. Dou, H-B. Yang and L. Xu designed the research and wrote the manuscript with assistance from the other authors. P.-P. Jia, Z.-Y. Peng, Y.-X. Hu, D.-Y. Zhang designed and analysed the experimental studies.

# Conflicts of interest

There are no conflicts to declare.

# Acknowledgements

This work was supported by the National Nature Science Foundation of China (no. 22107028 and 22103062), Program of Shanghai Outstanding Academic Leaders (no. 21XD1421200), Science and Technology Commission of Shanghai Municipality (22JC1403900), Shanghai Pujiang Program (no. 22PJ1402800), and the Fundamental Research Funds for the Central Universities, and the Open Research Fund of Shanghai Key Laboratory of Green Chemistry and Chemical Processes.

## References


1 N. S. Lewis and D. G. Nocera, *Proc. Natl. Acad. Sci. U. S. A.*, 2006, **103**, 15729.

2 (*a*) G. McDermott, S. M. Prince, A. A. Freer, A. M. Hawthornthwaite-Lawless, M. Z. Papiz, R. J. Cogdell and N. W. Isaacs, *Nature*, 1995, **374**, 517; (*b*) A. Melis, *Energy Environ. Sci.*, 2012, **5**, 5531.

3 (*a*) J. Barber, *Chem. Soc. Rev.*, 2009, **38**, 185; (*b*) T. Mirkovic, E. E. Ostroumov, J. M. Anna, R. van Grondelle, Govindjee and G. D. Scholes, *Chem. Rev.*, 2017, **117**, 249.

4 (*a*) S. Kundu and A. Patra, *Chem. Rev.*, 2017, **117**, 712; (*b*) G. D. Scholes, G. R. Fleming, A. Olaya-Castro and R. van Grondelle, *Nat. Chem.*, 2011, **3**, 763.

5 (*a*) R. Croce and H. van Amerongen, *Nat. Chem. Biol.*, 2014, **10**, 492; (*b*) P. D. Frischmann, K. Mahata and F. Wurthner, *Chem. Soc. Rev.*, 2013, **42**, 1847.

6 (*a*) Y. Wang, H. Suzuki, J. Xie, O. Tomita, D. J. Martin, M. Higashi, D. Kong, R. Abe and J. Tang, *Chem. Rev.*, 2018, **118**, 5201; (*b*) G. J. Hedley, A. Ruseckas and I. D. Samuel, *Chem. Rev.*, 2017, **117**, 796; (*c*) H. Q. Peng, L. Y. Niu, Y. Z. Chen, L. Z. Wu, C. H. Tung and Q. Z. Yang, *Chem. Rev.*, 2015, **115**, 7502; (*d*) M. Hao, G. Sun, M. Zuo, Z. Xu, Y. Chen, X. Y. Hu and L. Wang, *Angew. Chem., Int. Ed.*, 2020, **59**, 10095; (*e*) X. M. Chen, Q. Cao, H. K. Bisoyi, M. Wang, H. Yang and Q. Li, *Angew. Chem., Int. Ed.*, 2020, **59**, 10493; (*f*) K. Acharyya, S. Bhattacharyya, H. Sepehrpour, S. Chakraborty, S. Lu, B. Shi, X. Li, P. S. Mukherjee and P. J. Stang, *J. Am. Chem. Soc.*, 2019, **141**, 14565; (*g*) A. Kumar, R. Saha and P. S. Mukherjee, *Chem. Sci.*, 2021, **12**, 5319; (*h*) Z. Zhang, Z. Zhao, Y. Hou, H. Wang, X. Li, G. He and M. Zhang, *Angew. Chem., Int. Ed.*, 2019, **58**, 8862; (*i*) F. Wurthner, C. C. You and C. R. Saha-Moller, *Chem. Soc. Rev.*, 2004, **33**, 133; (*j*) A. Sautter, B. K. Kaletaş, D. G. Schmid, R. Dobrawa, M. Zimine, G. Jung, I. H. M. van Stokkum, L. De Cola, R. M. Williams and F. Würthner, *J. Am. Chem. Soc.*, 2005, **127**, 6719; (*k*) C. C. You, C. Hippius, M. Grune and F. Würthner, *Chem. – Eur. J.*, 2006, **12**, 7510; (*l*) Y.-X. Hu, P.-P. Jia, C.-W. Zhang, X.-D. Xu, Y. Niu, X. Zhao, Q. Xu, L. Xu and H.-B. Yang, *Org. Chem. Front.*, 2021, **8**, 5250; (*m*) G. Sun, W. Qian, J. Jiao, T. Han, Y. Shi, X.-Y. Hu and L. Wang, *J. Mater. Chem. A*, 2020, **8**, 9590; (*n*) C.-L. Sun, H.-Q. Peng, L.-Y. Niu, Y.-Z. Chen, L.-Z. Wu, C.-H. Tung and Q.-Z. Yang, *Chem. Commun.*, 2018, **54**, 1117; (*o*) H. Liu, Z. Zhang, C. Mu, L. Ma, H. Yuan, S. Ling, H. Wang, X. Li and M. Zhang, *Angew. Chem., Int. Ed.*, 2022, **61**, e202207289; (*p*) Y. Li, Y. Dong, L. Cheng, C. Qin, H. Nian, H. Zhang, Y. Yu and L. Cao, *J. Am. Chem. Soc.*, 2019, **141**, 8412; (*q*) D. Zhang, W. Yu, S. Li, Y. Xia, X. Li, Y. Li and T. Yi, *J. Am. Chem. Soc.*, 2021, **143**, 1313; (*r*) W.-J. Li, X.-Q. Wang, D.-Y. Zhang, Y.-X. Hu, W.-T. Xu, L. Xu, W. Wang and H.-B. Yang, *Angew. Chem., Int. Ed.*, 2021, **60**, 18761; (*s*) Y. Xia, M. Chen, S. Li, M. Li, X. Li, T. Yi and D. Zhang, *J. Mater. Chem. C*, 2022, **10**, 12332; (*t*) Z. Liu, X. Sun, X. Dai, J. Li, P. Li and Y. Liu, *J. Mater. Chem. C*, 2021, **9**, 1958.

7 F. Biedermann, E. Elmalem, I. Ghosh, W. M. Nau and O. A. Scherman, *Angew. Chem., Int. Ed.*, 2012, **51**, 7739.

8 (*a*) Y. H. Jeong, M. Son, H. Yoon, P. Kim, D. H. Lee, D. Kim and W. D. Jang, *Angew. Chem., Int. Ed.*, 2014, **53**, 6925; (*b*) P. Parkinson, C. E. Knappke, N. Kamonsutthipaijit, K. Sirithip, J. D. Matichak, H. L. Anderson and L. M. Herz, *J. Am. Chem. Soc.*, 2014, **136**, 8217; (*c*) J. Yang, M. C. Yoon, H. Yoo, P. Kim and D. Kim, *Chem. Soc. Rev.*, 2012, **41**, 4808; (*d*) R. Ziessel, G. Ulrich, A. Haefele and A. Harriman, *J. Am. Chem. Soc.*, 2013, **135**, 11330.

9 (*a*) L. B. Meng, D. Li, S. Xiong, X. Y. Hu, L. Wang and G. Li, *Chem. Commun.*, 2015, **51**, 4643; (*b*) Z. Xu, S. Peng, Y. Y. Wang, J. K. Zhang, A. I. Lazar and D. S. Guo, *Adv. Mater.*, 2016, **28**, 7666; (*c*) H. Q. Peng, J. F. Xu, Y. Z. Chen, L. Z. Wu, C. H. Tung and Q. Z. Yang, *Chem. Commun.*, 2014, **50**, 1334.

10 (*a*) H. Lee, Y. H. Jeong, J. H. Kim, I. Kim, E. Lee and W. D. Jang, *J. Am. Chem. Soc.*, 2015, **137**, 12394; (*b*) H.-Q. Peng, C.-L. Sun, L.-Y. Niu, Y.-Z. Chen, L.-Z. Wu, C.-H. Tung and Q.-Z. Yang, *Adv. Funct. Mater.*, 2016, **26**, 5483; (*c*) C. D. Bosch, S. M. Langenegger and R. Haner, *Angew. Chem., Int. Ed.*, 2016, **55**, 9961; (*d*) X. Ban, T. Zhou, Q. Cao, K. Zhang, Z. Tong, H. Xu, A. Zhu and W. Jiang, *J. Mater. Chem. C*, 2022, **10**, 15114.

11 (*a*) A. Ajayaghosh, V. K. Praveen, C. Vijayakumar and S. J. George, *Angew. Chem., Int. Ed.*, 2007, **46**, 6260; (*b*) A. Del Guerzo, A. G. Olive, J. Reichwagen, H. Hopf and J. P. Desvergne, *J. Am. Chem. Soc.*, 2005, **127**, 17984; (*c*) C. Felip-León, S. Díaz-Oltra, F. Galindo and J. F. Miravet, *Chem. Mater.*, 2016, **28**, 7964; (*d*) K. V. Rao, K. K. Datta, M. Eswaramoorthy and S. J. George, *Angew. Chem., Int. Ed.*, 2011, **50**, 1179; (*e*) R. Sethy, J. Kumar, R. Metivier, M. Louis, K. Nakatani, N. M. T. Mecheri, A. Subhakumari, K. G. Thomas, T. Kawai and T. Nakashima, *Angew. Chem., Int. Ed.*, 2017, **56**, 15053.

12 (*a*) P. K. Dutta, S. Levenberg, A. Loskutov, D. Jun, R. Saer, J. T. Beatty, S. Lin, Y. Liu, N. W. Woodbury and H. Yan, *J. Am. Chem. Soc.*, 2014, **136**, 16618; (*b*) F. Garo and R. Haner, *Angew. Chem., Int. Ed.*, 2012, **51**, 916; (*c*) L. Zhao, H. Zou, H. Zhang, H. Sun, T. Wang, T. Pan, X. Li, Y. Bai, S. Qiao, Q. Luo, J. Xu, C. Hou and J. Liu, *ACS Nano*, 2017, **11**, 938; (*d*) Q. Zou, K. Liu, M. Abbas and X. Yan, *Adv. Mater.*, 2016, **28**, 1031.

13 (*a*) M. E. Foster, J. D. Azoulay, B. M. Wong and M. D. Allendorf, *Chem. Sci.*, 2014, **5**, 2081; (*b*) V. M. Suresh, S. J. George and T. K. Maji, *Adv. Funct. Mater.*, 2013, **23**, 5585; (*c*) X. Zhang, M. A. Ballem, Z. J. Hu, P. Bergman and K. Uvdal, *Angew. Chem., Int. Ed.*, 2011, **50**, 5729; (*d*) S. Bhattacharyya, B. Jana and A. Patra, *ChemPhysChem*, 2015, **16**, 796.

14 (*a*) L. Ji, Y. Sang, G. Ouyang, D. Yang, P. Duan, Y. Jiang and M. Liu, *Angew. Chem., Int. Ed.*, 2019, **58**, 844; (*b*) X. Wei, X. Su, P. Cao, X. Liu, W. Chang, M. Li, X. Zhang and Z. Liu, *Nature*, 2016, **534**, 69.


 

15 (*a*) D. Yang, P. Duan, L. Zhang and M. Liu, *Nat. Commun.*, 2017, **8**, 15727; (*b*) Z. Xu, D. Gonzalez-Abradelo, J. Li, C. A. Strassert, B. J. Ravoo and D.-S. Guo, *Mater. Chem. Front.*, 2017, **1**, 1847; (*c*) S. Afzal, M. S. Lone, P. A. Bhat and A. A. Dar, *J. Photochem. Photobiol., A*, 2018, **365**, 220; (*d*) L. Xu, Z. Wang, R. Wang, L. Wang, X. He, H. Jiang, H. Tang, D. Cao and B. Z. Tang, *Angew. Chem., Int. Ed.*, 2020, **59**, 9908.

16 (*a*) J. Luo, Z. Xie, J. W. Lam, L. Cheng, H. Chen, C. Qiu, H. S. Kwok, X. Zhan, Y. Liu, D. Zhu and B. Z. Tang, *Chem. Commun.*, 2001, 1740; (*b*) Y. Sun and P. J. Stang, *Aggregate*, 2021, **2**, e94; (*c*) Z. Zhao, Z. Wang, J. Tavakoli, G. Shan, J. Zhang, C. Peng, Y. Xiong, X. Zhang, T. S. Cheung, Y. Tang, B. Huang, Z. Yu, J. W. Y. Lam and B. Z. Tang, *Aggregate*, 2021, **2**, e36; (*d*) L. Wang, S. Xin, F. Xie, X. Ran, H. Tang and D. Cao, *J. Mater. Chem. C*, 2022, **10**, 14605.

17 (*a*) C. Bannwarth, S. Ehlert and S. Grimme, *J. Chem. Theory Comput.*, 2019, **15**, 1652; (*b*) M. Bursch, H. Neugebauer and S. Grimme, *Angew. Chem., Int. Ed.*, 2019, **58**, 11078.

18 W. Humphrey, A. Dalke and K. Schulten, *J. Mol. Graphics*, 1996, **14**, 33.

19 T. Lu and F. Chen, *J. Comput. Chem.*, 2012, **33**, 580.

20 (*a*) W. F. Watson and R. Livingston, *J. Chem. Phys.*, 1950, **18**, 802; (*b*) G. S. Beddard and G. Porter, *Nature*, 1976, **260**, 366; (*c*) H. Narita, L. Catti and M. Yoshizawa, *Angew. Chem., Int. Ed.*, 2021, **60**, 12791; (*d*) S. Sekiguchi, K. Kondo, Y. Sei, M. Akita and M. Yoshizawa, *Angew. Chem., Int. Ed.*, 2016, **55**, 6906; (*e*) K. Omoto, S. Tashiro and M. Shionoya, *J. Am. Chem. Soc.*, 2021, **143**, 5406.

21 (*a*) M. Xue, Y. Yang, X. Chi, Z. Zhang and F. Huang, *Acc. Chem. Res.*, 2012, **45**, 1294; (*b*) Z. Y. Li, Y. Zhang, C. W. Zhang, L. J. Chen, C. Wang, H. Tan, Y. Yu, X. Li and H.-B. Yang, *J. Am. Chem. Soc.*, 2014, **136**, 8577.